ACS APPLIED MATERIALS & INTERFACES

Research Article

www.acsami.org

Nanoscale Rings from Silicon-Containing Triblock Terpolymers

Marc D. Rodwogin,[†,‡] A. Baruth,[‡,§] Elizabeth A. Jackson,[†] C. Leighton,[§] and Marc A. Hillmyer*[,†]

[†]Department of Chemistry and [§]Department of Chemical Engineering and Material Science, University of Minnesota, Minneapolis, Minnesota 55455, United States

Supporting Information

ABSTRACT: Nanoscopic ring arrays of various materials show promise for both technological applications and fundamental studies. In this work we report the preparation of sub-50 nm diameter ring arrays from metallic thin films using a block polymer lithographic pattern transfer approach. We prepared a triblock terpolymer that adopts a core−shell cylindrical morphology where the shell is an oxidizable polydimethylsiloxane block. Solvent annealed thin films of this terpolymer produce cylindrical features oriented perpendicular to the substrate surface. The polydimethylsiloxane shell is then converted into SiO_x rings by an oxygen reactive ion etch. The resultant hard mask pattern is then transferred into Au, $Ni_{80}Fe_{20}$, and $Ni_{80}Cr_{20}$ thin films via Ar ion beam milling, demonstrating the generality of the approach.

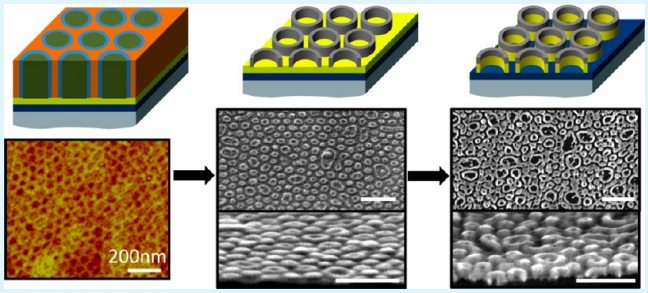

KEYWORDS: *triblock terpolymer, PDMS, cylinder, nanoring, solvent annealing, block polymer, ring array*

INTRODUCTION

Diblock copolymers containing two immiscible, covalently bound segments are an interesting class of self-assembling soft materials.[1,2] The simplest example, a linear AB diblock, can self-assemble into spherical, cylindrical, bicontinuous gyroid, or lamellar morphologies at the nanoscale, depending primarily on the relative size of each segment and their degree of incompatibility.[3] Through pattern transfer strategies using thin films of microphase separated AB diblock copolymers, ordered arrays of nanoscale dots, lines, holes, or trenches with areal densities on the order of 1×10^{11} to 1×10^{12} features per square inch have been achieved.[4] However, without additional, and often complex, lithographic steps, AB diblock polymers are limited to these simple topographical features.[5] ABC triblock terpolymers on the other hand, provide additional degrees of freedom and are capable of adopting significantly more diverse morphologies,[1] such as core−shell cylinders.[6,7] Such a morphology lends itself, via similar transfer techniques used in diblock systems, to the fabrication of nanoscale rings and antirings that are attractive for the study of fundamental phenomena such as persistent currents in metals[8,9] and new micromagnetic ground states and excitations in ferromagnets,[10,11] in addition to potential applications in chemical sensing.[12,13] The majority of nanoring arrays reported in the literature have been prepared using colloidal,[12,14] e-beam,[10,15] or nanoimprint lithography,[16] whereas the use of self-assembled microphase separated block polymers as lithographic templates for this purpose has received much less attention.[17] An overview of the attempts to employ block polymers in this capacity is given below. In this work, we present a new strategy for nanoring array formation that utilizes a core−shell cylindrical morphology, derived from a triblock terpolymer. A polydimethylsiloxane (PDMS) core−shell is converted into SiO_x rings by an oxygen reactive ion etch and serves as a hard mask for subsequent patterning into disparate materials.

We briefly review here some of the more exotic approaches for producing arrays of nanorings using block polymers. First, the use of polystyrene-*b*-poly(4-vinyl pyridine) swollen with 2,4-hydroxybenzeneazonebzoic acid (HABA) resulted in the formation of weakly ordered carbon nanoring arrays using a multistep approach of HABA removal and subsequent selective dewetting of a carbon precursor.[18] Second, nanoscopic TiO_2 rings were produced from an amphiphilic dendrimer containing a polyphenylene core with 12 PS-*b*-poly(acrylic acid) (PAA) arms.[19] Complexing the PAA domains with titanium isopropoxide, followed by calcination to remove the polymer, left rings of TiO_2 with dimensions similar to those of the dendrimers. Finally, PS-*b*-poly(2-vinyl pyridine) (P2VP)-based micelles have been used to prepare gold nanorings.[20] In this approach, reverse micelles were prepared by dissolving the block polymer in *o*-xylene, a PS-selective solvent, followed by spin-coating of the micelle solution onto a Si substrate. The micellar film was exposed to a solution of $HAuCl_4$ and HCl, which resulted in a core−corona inversion. Subsequent reduction of the $HAuCl_4$ in an oxygen plasma resulted in an array of gold nanorings.

Considering more direct diblock copolymer lithographic approaches, deposition of Co at a grazing angle into a rotating nanoporous PS thin film array, derived from degraded PS-*b*-poly(methyl methacrylate) (PMMA), generated Co nanorings

Received: April 6, 2012
Accepted: June 19, 2012
Published: July 3, 2012

upon ion beam etching.[21] Next, using PS-*b*-poly(ethylene oxide) (PEO) containing a disulfide bond at the PS-*b*-PEO juncture, well-ordered thin films containing PEO cylinders in a PS matrix were obtained after solvent annealing.[22] Cleavage of the disulfide bond with D,L-dithiothreitol resulted in a nanoporous PS matrix with thiol-lined pores, where subsequent complexation of $HAuCl_4$ with the latent thiol groups, followed by reduction of the gold salt with hydrazine, lead to a ring-shaped array of gold nanoparticles localized at the pore walls within the PS matrix. Finally, PS-*b*-PDMS was used to fabricate an array of silicon oxy-carbide rings.[23] A thin film of PS-*b*-PDMS was solvent annealed to form a well-ordered array of surface perpendicular PDMS cylinders in a PS matrix. Dodecane immersion triggered a surface reconstruction event, where subsequent generation of a PS film containing cylindrical nanopores lined with a PDMS brush layer was the result. Exposing this film to an oxygen reactive ion etch (O_2 RIE) oxidized the PDMS chains and removed the residual PS, yielding an array of silicon oxy carbide rings.

In addition to diblock polymers, as discussed above, a few approaches using triblock terpolymers for nanoring syntheses have also been reported. First, a thin film of core−shell cylinder forming poly(isoprene)-PS-poly(lactide) (PI-PS-PLA) resulted in PS nanorings following ozonolysis of the PI matrix and basic etching of the PLA core.[7] A similar approach was executed with PMMA-PS-poly(butadiene) (PB) ABC triblock polymer in which the PMMA formed the cylinder core, wrapped in a PS core−shell, all within a PB matrix.[24] The PMMA core was removed using UV irradiation and O_2 RIE, whereas the PB matrix was removed with ozone and UV irradiation. In this case, the resulting PS nanoring template was transferred into a SiO_2 underlayer using a CHF_3 RIE, with only about 20% of the ring features effectively being transferred. Next, Fe nanorings were produced from a PS-P2VP-PEO triblock polymer.[25] Exposure of a film of PS-P2VP-PEO to $FeCl_3$, followed by reduction of the salt, led to the formation of iron nanorings. Finally, the triblock terpolymer PS-b-poly(ferrocenylsilane)-b-P2VP (PS-PFS-P2VP) was used to fabricate metal oxide nanoring arrays.[26] This block polymer formed a core−shell cylindrical morphology, with the PS domains as the cylinder core, PFS as the core−shell, and P2VP as the matrix. The PFS domains contain both iron and silicon atoms in the polymer backbone, thus exposure of surface perpendicularly aligned core−shell cylinders to an O_2 RIE etched both the PS and P2VP domains and simultaneously oxidized the PFS domains into the corresponding metal oxide ring. In this result, cross-sectional scanning electron microscopy (SEM) images showed that the perpendicular cylinders did not span the entire film thickness, and the resulting rings transitioned to a surface parallel orientation near the substrate, precluding it from direct pattern transfer. However, it was successfully demonstrated as a nanoimprint lithography mold.

In the preceding examples, not only are the methods generally complex, but the successful transfer of the polymer nanoring arrays into disparate materials using a simple, top-down (i.e., subtractive) approach was either challenging or in many cases unsuccessful. This is due to either the typically poor etch contrast of the individual blocks with most inorganic materials, or the failure of the cylindrical domains to span the entire film thickness. In this manuscript, we describe an approach that circumvents both of these difficulties via the use of a core−shell cylinder forming PS-PDMS-PLA ABC triblock terpolymer. Solvent annealing of a thin film of this material results in perpendicularly aligned core−shell cylindrical domains that span the entire film thickness. The PDMS midblock thus not only provides high etch contrast between the constituent blocks but also, upon O_2 RIE, produces a SiO_x nanoring template, i.e., a robust etch mask. This method thus allows for the direct fabrication of nanoring arrays in a variety of disparate materials using only established dry etching techniques (e.g., Ar ion beam milling). In this work, we successfully demonstrate pattern transfer into Au, NiFe, and NiCr. These materials are interesting, as they represent two ends of the spectrum for etch rates of metals via Ar ion beam milling (i.e., Au mills very fast (10 nm/min) and NiFe and NiCr very slowly (1−2 nm/min)). They are also very relevant in applications; Au nanorings can be used for sensing applications, while NiFe is a prototypical soft ferromagnetic alloy, exhibiting novel micromagnetic ground states in nanoring structures. Although this is related to past work on PS-PFS-P2VP,[26] the synthetic accessibility of PDMS as compared to PFS, in addition to the lateral ordering of the cylinders that traverse through the entire extent of the film, makes this approach attractive for direct production of nanoring arrays in a variety of materials.

METHODS

Reagents and Syntheses. Styrene and hexamethylcyclotrisiloxane (D3) were purchased from Aldrich and distilled twice prior to use. Allyl alcohol and chlorodimethylsilane were also distilled once prior to use. *d*,*l*-lactide was purchased from Purac, and was crystallized from ethyl acetate and dried in vacuo at room temperature prior to polymerization. Sec-butyl lithium (Aldrich), Karstedt's Catalyst (Gelest) and triethyl aluminum (Aldrich) were used without purification. Cyclohexane, tetrahydrofuran (THF), and toluene were purified on a home-built solvent purification system via passage over a molecular sieve column and an activated alumina column. THF, in addition to purification on a home-built solvent column, was distilled prior to use. All other solvents were reagent grade and were used without further purification.

The preparation of silane terminated PS-PDMS was carried out via sequential anionic polymerization techniques. To begin, 250 mL of cyclohexane was added to a 2 L, 5-neck round-bottom flask equipped with a stir bar. The reaction flask was evacuated and refilled with dry Ar(g) three times prior to the addition of 250 mL of cyclohexane and 2 mL of (2.8×10^{-4} mol) sec-butyl lithium. Styrene, 5.0 g (4.8×10^{-2} mol), was added to this initiator solution, which caused the reaction to turn red. After 4 h of stirring at 40 °C, D3 was added to the reaction and the temperature was reduced to 25 °C. Addition of the D3 monomer caused the red color of the reaction to fade. After 9 h, complete crossover from the polystyryl anion to the polystyrene-polydimethylsiloxyl anion was obtained, and 250 mL of distilled THF was added to the reaction mixture. D3 was polymerized for an additional 1.75 h before 2.8 mL (2.5×10^{-2} mol) chlorodimethylsilane was added to terminate the reaction.[27] After termination, the reaction was washed once with a 5% $NaHCO_3$ solution and three times with DI water before precipitation into 1.5 L of a 50:50 solution of methanol and isopropanol.

In a typical hydrosilylation reaction, 0.500 g (1.3×10^{-5} mol) PS-PDMS-H was added to a high-pressure vessel equipped with a stir bar. Toluene was added (2 mL) and the solution was allowed to stir until the polymer was completely dissolved. To the reaction mixture was added 0.095 mL (1.3×10^{-3} mol) of allyl alcohol and 0.010 mL (1.00×10^{-6} mol) of Karsedt's catalyst. The reaction was stirred at 90 °C for 24 h before being allowed to cool to room temperature, diluted with dichloromethane, and precipitated in methanol.

The final PS-PDMS-PLA was prepared in a dry pressure vessel equipped with a stir bar and charged with 0.289 g (7.6×10^{-6} mol) PS-PDMS−OH. The reaction was then moved into a drybox, where 3 mL of toluene and 0.04 mL (3.8×10^{-6} mol) of triethyl aluminum in

hexanes was added.[28,29] The reaction was allowed to stir overnight at room temperature before 0.169 g (1.18×10^{-3} mol) of *d*,*l*-lactide was added. The reaction was transferred from the drybox into an oil bath and stirred at 90 °C. After 24 h, the reaction was allowed to cool to room temperature, terminated with approximately 2 mL of 1 M HCl(aq) and precipitated in methanol. After drying the reaction in vacuo, residual PS-PDMS was extracted from the triblock polymer via washing with cold cyclohexane and centrifugation.

Thin Film Preparation. Thin films of PS-PDMS-PLA were prepared from solutions in chlorobenzene at a concentration of 20 mg/mL (approximately 2% by weight). Polymer solutions were spin-coated at 2000 rpm for 30 s onto the chosen substrate (detailed in manuscript). The metallic film substrates were produced via dc magnetron sputtering from composite metal targets ($Ni_{80}Fe_{20}$ and $Ni_{80}Cr_{20}$) and a Au target, where the Si substrate was degreased under sonication prior to deposition in acetone followed by methanol. Films were solvent annealed in a drybox with toluene vapor by placing a 10 mL dish of solvent into a 500 mL sealed glass container with the film placed inside on a pedestal just above the liquid solvent. Termination of the annealing was achieved by removing the lid to the sealed glass container and quickly removing the film.

Reactive ion etching experiments using both O_2 and CF_4 were performed on a Model 320 batch plasma etcher made by Surface Technology Systems. O_2 RIE experiments were done at a process pressure of 3×10^{-2} Torr and a chamber power of 50 W. CF_4 RIE experiments were performed with a process pressure and power of 3×10^{-2} Torr and 60 W, respectively. Ar ion beam milling experiments were performed on a Technics Argon Ion Mill using a process pressure of 8×10^{-5} Torr, an accelerating voltage of 100 V, and an ion beam current of 85 mA.

Characterization. ^{1}H NMR spectra were obtained on Varian INOVA-300, VXR-300, or INOVA-500 spectrometers in $CDCl_3$ at room temperature. Samples were prepared by dissolving approximately 20 mg of polymer in approximately 0.700 mL of deuterated chloroform. Each spectrum was obtained after 32 scans with a 20 s pulse delay. Size exclusion chromatography (SEC) was performed on an Agilent 1100 series instrument equipped with an HP 1047A refractive index detector. Three PLgel Mixed C Columns as well as a PLgel 5 μm guard column from Varian were employed. Chloroform was used as the mobile phase at 35 °C flowing at a rate of 1 mL/min. Polymer samples were prepared at an approximate concentration of 0.3% (wt:wt) in chloroform. Molecular weights were determined from calibrated curves created from narrow molar mass distribution PS standards purchased from Polymer Laboratories. Transmission electron microscopy images were obtained on a Jeol-JEM 1210 operating at an accelerating voltage of 120 kV. Samples were prepared by drop casting from a solution in THF (0.01% by wt.) onto carbon-coated TEM grids with the intention of imaging the "as-cast" morphology cf. a microtomed bulk monolith. The resulting film was sufficiently thin for transmission imaging, and the observed morphology was uniform across the various imaged areas (two are shown in Figure 2a, b). Small angle X-ray synchrotron scattering (SAXS) data was obtained at Argonne National Laboratory, using an X-ray wavelength of 0.8856 Å and a sample-to-detector distance of 4 m. Powder samples were packed into hermetic differential scanning calorimetry pans and sealed with Kapton tape. Two-dimensional scattering rings were azimuthally integrated to obtain plots of intensity versus the scattering wave vector *q*. Polymer film thickness was determined by spectroscopic ellipsometry (J.A. Wollam Co., Inc.) and metal thickness by grazing incidence X-ray reflectivity (Panalytical X'Pert Pro). Tapping mode atomic force microscopy was performed on a Digital Instruments Nanoscope III microscope using engagement set points between 0.9 − 0.95 of the free amplitude oscillation. Scanning electron microscopy was performed on a Hitachi S900 FE-SEM using an accelerating voltage between 3.0 and 5.0 kV.

RESULTS AND DISCUSSION

The synthesis of the PS-PDMS-PLA triblock polymer was carried out according to Figure 1. Briefly, silane-terminated PS-PDMS was synthesized by sequential anionic polymerization of styrene and hexamethyltrisiloxane (D3), followed by end-capping with chlorodimethylsilane.[27] Hydrosilylation of the terminal silane with allyl alcohol was carried out using Karstedt's catalyst to install a terminal hydroxyl group that was subsequently used for the triethyl aluminum-catalyzed polymerization of lactide.[28,29]

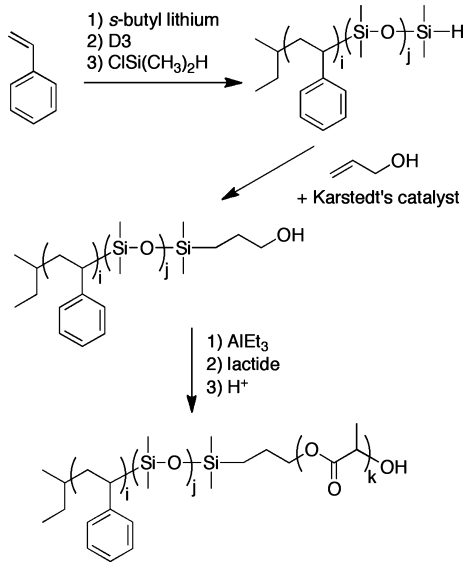

Figure 1. Synthetic scheme for the preparation of PS-PDMS-PLA.

The successful synthesis of the block polymer was confirmed using both ^{1}H NMR spectroscopy and size exclusion chromatography (SEC). Disappearance of the terminal silane proton in the ^{1}H NMR spectra and concurrent appearance of the methylene protons adjacent to the terminal hydroxyl of the hydroxyl functionalized PS-PDMS is consistent with the installation of a terminal hydroxyl group (see Supporting Information). A downfield shift of those protons upon the formation of PS-PDMS-PLA is consistent with growth of PLA to form the triblock terpolymer. SEC data on the triblock terpolymer relative to the hydroxyl terminated PS-PDMS gave a monomodal peak at a lower elution volume, also corroborating successful triblock polymer formation. Both the PS-PDMS-H and PS-PDMS−OH SEC traces show a small high molecular weight shoulder, which is believed to correspond to coupled material (PS-PDMS-PS). This undesired product was extracted with cold cyclohexane after the final PLA synthesis and was not observed in the SEC trace of the PS-PDMS-PLA used in the subsequent studies. From the ^{1}H NMR spectra the molar masses for PS-PDMS-PLA were determined for the PS block (33 kg mol^{-1}), PDMS block (7 kg mol^{-1}) and PLA block (25 kg mol^{-1}). A polydispersity index for this PS-PDMS-PLA triblock of 1.16 was determined by SEC, with volume fractions $f_{PS} = 0.54$, $f_{PDMS} = 0.12$ and $f_{PLA} = 0.34$. (SEC traces and ^{1}H NMR spectra details are provided in the Supporting Information). The molar masses for each block were chosen based on prior work with PS-PI-PLA,[7] which adopted a core−shell cylindrical microstructure in a similar compositional range. As shown below, this composition does adopt the anticipated morphology. The insensitivity to exact composition is likely due to the limited length of the PDMS chains, similar to PS-PI-PLA. Given our initial success in accessing this microstructure, the present investigation was carried out for this composition without further optimization.

X-ray scattering experiments at the Advanced Photon Source at Argonne National Lab, as well as bright-field transmission electron microscopy (TEM), were used to characterize the bulk morphology of this system, and are shown in Figure 2. TEM

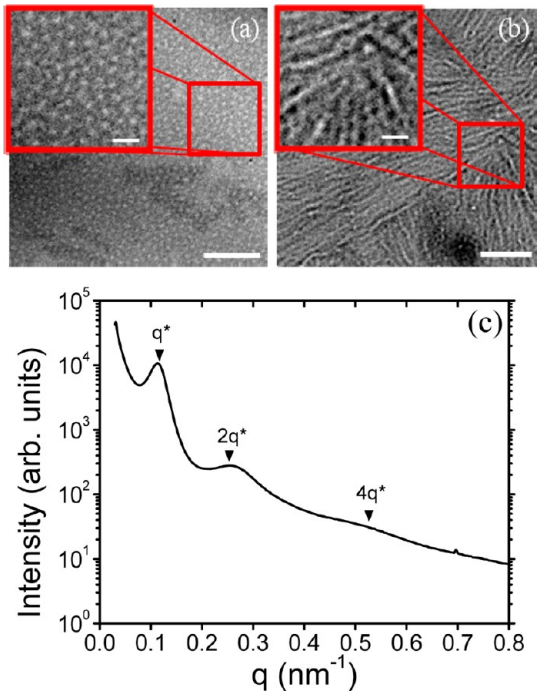

Figure 2. Bright-field TEM images of cylindrical PS-PDMS-PLA with the cylinder long axes oriented (a) parallel and (b) perpendicular to the electron beam. Scale bars represent 400 nm in the low magnification image and 100 nm in the high magnification insets. (c) 1D SAXS trace showing strong principal scattering peak, q^*, and two additional peaks at approximately $2q^*$ and $4q^*$. Arrowheads show predicted peak positions based on principal reflection.

images indicate cylinders of PLA (white) sheathed in PDMS (black), within a PS matrix (gray), with their long axes oriented parallel (Figure 2a) and perpendicular (Figure 2b) to the electron beam, consistent with a core−shell cylindrical microstructure. Small-angle X-ray scattering (SAXS) on an unaligned powder sample (Figure 2c) showed a strong principal scattering peak, q^*, and two higher order reflections at approximately $2q^*$ and $4q^*$. From the location of the principal scattering peak, we extract a domain spacing of ∼54 nm. Although no generic morphology map exists for the ABC triblock polymers, as it does for AB diblock polymers,[1] based on analogy with PS-PI-PLA these volume fractions are expected to adopt a hexagonally close-packed, core−shell cylindrical microstructure.[6,7] Therefore, this domain spacing corresponds to a center-to-center distance of 62 nm, an inner core diameter of 38 nm, an outer core diameter of 45 nm, and a shell thickness of 3.5 nm.

A thin film of PS-PDMS-PLA was prepared from a 2 wt % solution in chlorobenzene by spin coating onto $Ni_{80}Cr_{20}$ (10 nm)/Au (10 nm) and $Ni_{80}Fe_{20}$ (10 nm)/Au (10 nm) films at 2000 rpm. The metallic films were dc magnetron sputtered onto naturally oxidized Si substrates from two sources ($Ni_{80}Cr_{20}$ or $Ni_{80}Fe_{20}$ and Au). Ellipsometric analysis of a polymer film prepared on a bare Si substrate gave an approximate thickness of 52 nm for this solution concentration and spinning speed. A representative tapping mode Atomic Force Microscopy (AFM) micrograph of this film is shown in Figure 3a. Both worm-like and circular features on the surface

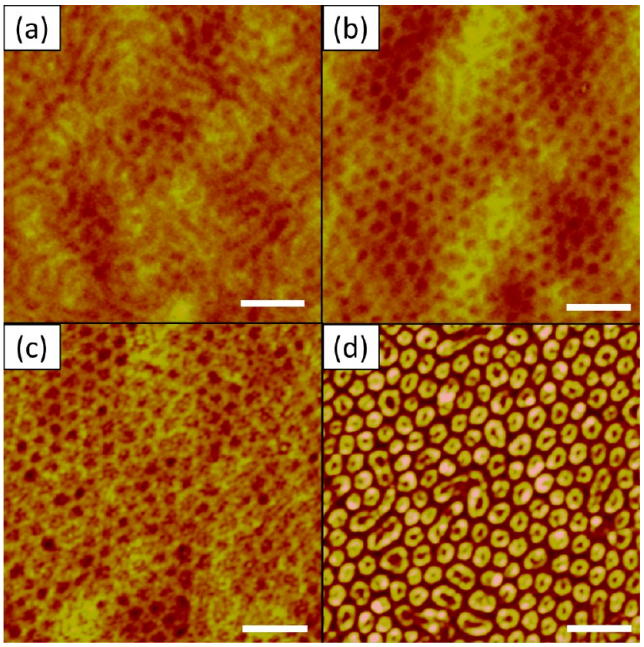

Figure 3. AFM tapping mode images of a 52 nm thick PS-PDMS-PLA film (a) as spun, (b) after solvent annealing (toluene, 60 min), (c) after 15 s CF_4 RIE, and (d) after 60 s O_2 RIE. Predominantly surface perpendicular cylinders are obtained after solvent annealing from a mixed orientation film. After short CF_4 and O_2 RIE steps, a nanoring array is observed. Horizontal scale bar is 200 nm and the height scale for all images is 10 nm.

of the film are apparent; this is consistent with a cylindrical microstructure where the cylinder long axes are oriented both perpendicular and parallel to the substrate. These circular features (corresponding to the outer core) measure approximately 43 ± 6 nm in diameter, and exhibit an approximate center-to-center spacing of 61 ± 8 nm, in good agreement with the SAXS data.[30]

Initially, we expected spontaneous perpendicular alignment of the core−shell cylinders based on recent results for PS-PI-PLA triblock terpolymer containing the low surface energy PI midblock.[31] In both systems, wetting of the low surface energy midblock (E_{surf}^{PI} = 32 mJ/m^2, E_{surf}^{PDMS} = 21 mJ/m^2 < $E_{surf}^{PS} \approx E_{surf}^{PLA}$ 40 mJ/m^2)[32,33] to the free surface is energetically favorable. However, in the PS-PI-PLA system in particular, the entropic penalty associated with looping of the PI midblock and the enthalpic penalty of forcing PS/PLA contacts (i.e., free surface PI brush layer) must be considered. All of these constraints are satisfied in the PS-PI-PLA case when the cylinders are aligned perpendicular to the surface, exposing all blocks to the free surface, combated only by the energy penalty associated with having PS and PLA at the free surface, which is apparently sufficiently small. It is clear from the current work that a similar argument cannot be made for the PS-PDMS-PLA system, likely due to the surface energy of PDMS being significantly lower than that of PI. In this case, the energetic gain that results from maximizing the area of the PDMS/air interface is larger and is seemingly comparable to the entropic and enthalpic penalties that were avoided in the PS-PI-PLA case. The end result is a PDMS wetting layer, described further below, thus avoiding PS and PLA contact with the free surface

resulting in a mixed orientation of cylinders parallel and perpendicular to the substrate. As discussed below, the orientation can, however, be controlled with the use of a solvent annealing treatment.

To improve the level of perpendicular orientation and degree of lateral order the PS-PDMS-PLA thin films were annealed in toluene vapor, a somewhat PS/PDMS selective solvent. This process causes swelling of the polymer blocks and mediation of their surface energies. In addition, it lowers the glass transition temperature (T_g) and increases mobility. In the case of a neutral solvent, the surface energy for all blocks then becomes comparable, producing an ordering front at the polymer/vapor interface that can favor perpendicular alignment of the cylinders, facilitate annealing of defects, and lead to strong lateral ordering that propagates through the bulk of the film as the solvent evaporates.[34,35] After exposing these films to toluene vapor for 60 min (Figure 3b), cylinders oriented normal to the substrate, with improved hexagonal order, were observed. However, the low surface energy PDMS continues to form a thin wetting layer at the free surface (as alluded to above and demonstrated below). From the tapping mode AFM image, outer-core diameters of 39 ± 5 nm and center-to-center distances of 61 ± 9 nm were obtained, again consistent with SAXS and AFM measurements on the as-spun film.

In initial experiments, due to the fact that we did not anticipate a PDMS wetting layer, the PS-PDMS-PLA films were exposed to a 60 s O_2 RIE to attempt to oxidize the PDMS to SiO_x and concurrently remove the PS and PLA. However, upon oxidation, narrow threads of SiO_x linking the oxidized PDMS domains were clearly observed (see Supporting Information). This result confirms our assertion made above regarding the existence of a PDMS surface wetting layer. The threads are attributed to the oxidation of this surface wetting layer. Such wetting layers have been observed previously by Jung and Ross, and were removed by exposing the film to a brief CF_4 RIE, having high selectivity toward silicon-containing materials.[36] Indeed, after a 15 s CF_4 RIE of the PS-PDMS-PLA films (Figure 3c), the dark circular features on the surface of the film are more clearly observed, again consistent with cylinders oriented perpendicular to the substrate, but now with the PDMS wetting layer removed.

On the basis of the confirmation of a thin PDMS wetting layer, a successful pattern template transfer strategy was employed, as shown in Figure 4. Incorporating this initial PDMS wetting layer removal step, thin films were then exposed to an O_2 RIE for 60 s (the only etch time investigated, based on known etch rates to fully remove both the PS and PLA blocks). The resulting AFM image (Figure 3d) shows an array of nanoscale rings with an inner-core diameter of 16 ± 6 nm, outer-core diameter of 50 ± 7 nm, and center-to-center distance of 61 ± 8 nm. Althouh the center-to-center distance is completely consistent with the pattern dimensions prior to the RIE processing steps, the outer-core diameter is 28% larger than the values obtained from AFM images of the film before O_2 RIE (50 cf. 39 nm). The corresponding shell thickness is also much larger than the shell thickness calculated from SAXS data (17 cf. 4 nm). However, the accuracy of these values may be limited by convolution with the AFM tip profile. From SEM (Figure 5a) the inner-core diameter is 24 ± 15 nm, resulting in a shell thickness of only 12 nm, more consistent with expectation based on the molar mass of the triblock, SAXS data, and spreading of the PDMS domain during oxidation (see below).

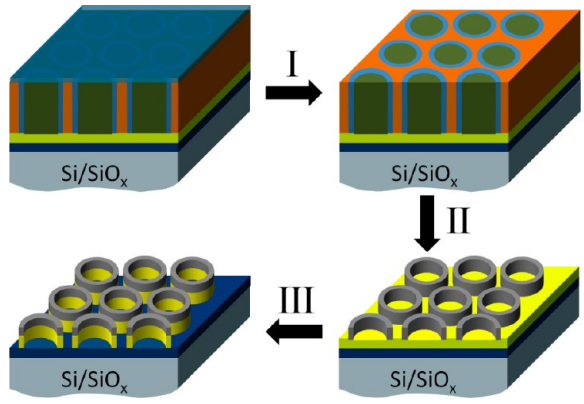

Figure 4. Cartoon of film processing. A thin film of PS-PDMS-PLA is first exposed to a short CF_4 RIE (I) to remove a thin PDMS surface wetting layer (blue), followed by O_2 RIE (II) to oxidize the PDMS (blue) domains and simultaneously remove the PS (orange) and PLA (green). The pattern of the remaining SiO_x rings (gray) was then transferred into the underlying capping material, Au (yellow), and continued through the lower alloy layer (blue) using Ar ion beam milling (III).

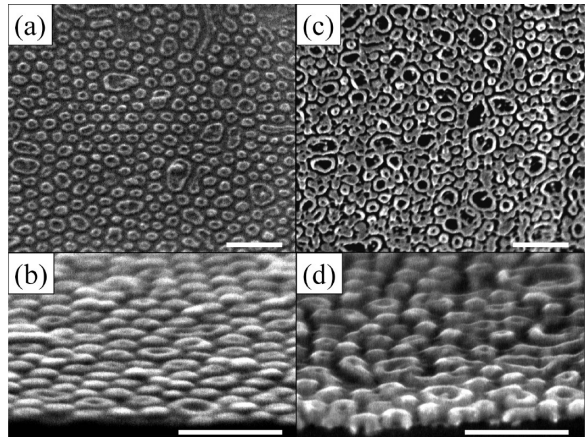

Figure 5. Plan view and cross-sectional view SEM images of the SiO_x ring array (a, b) before and (c, d) after pattern transfer into an underlying 10 nm Au layer. Unmasked Au was removed via normal incidence Ar ion beam milling, leaving gold rings capped with residual SiO_x mask. The inner and outer diameters of the rings after milling are consistent with those before milling. A height increase of approximately 11 nm is observed, roughly consistent with the thickness of the Au underlayer. Cross-sectional images were obtained by cryogenically fracturing specimens in liquid N_2. Scale bars are 200 nm.

In addition to an observed increase in shell thickness, it is apparent that the dispersion in size and shape is somewhat modified between the images taken before (Figure 3b,c) and after (Figure 3d) the oxidation step. The observed ring expansion, ellipticity increase, and coupling with adjacent features may be due to spreading of the PDMS domains during oxidation as well as a residual PDMS surface layer. Further optimization of the CF_4 and O_2 RIE may yield a more consistent feature size and shape. From a cross sectional SEM image of the oxidized film (Figure 5b), the height of the SiO_x rings is approximately 11 nm. If the rings were to maintain the same lateral area during oxidation, then taking into account the literature density of PDMS (0.98 g/cm^3)[37] and amorphous SiO_2 (2.2 g/cm^3)[38] (and assuming this density is similar to our

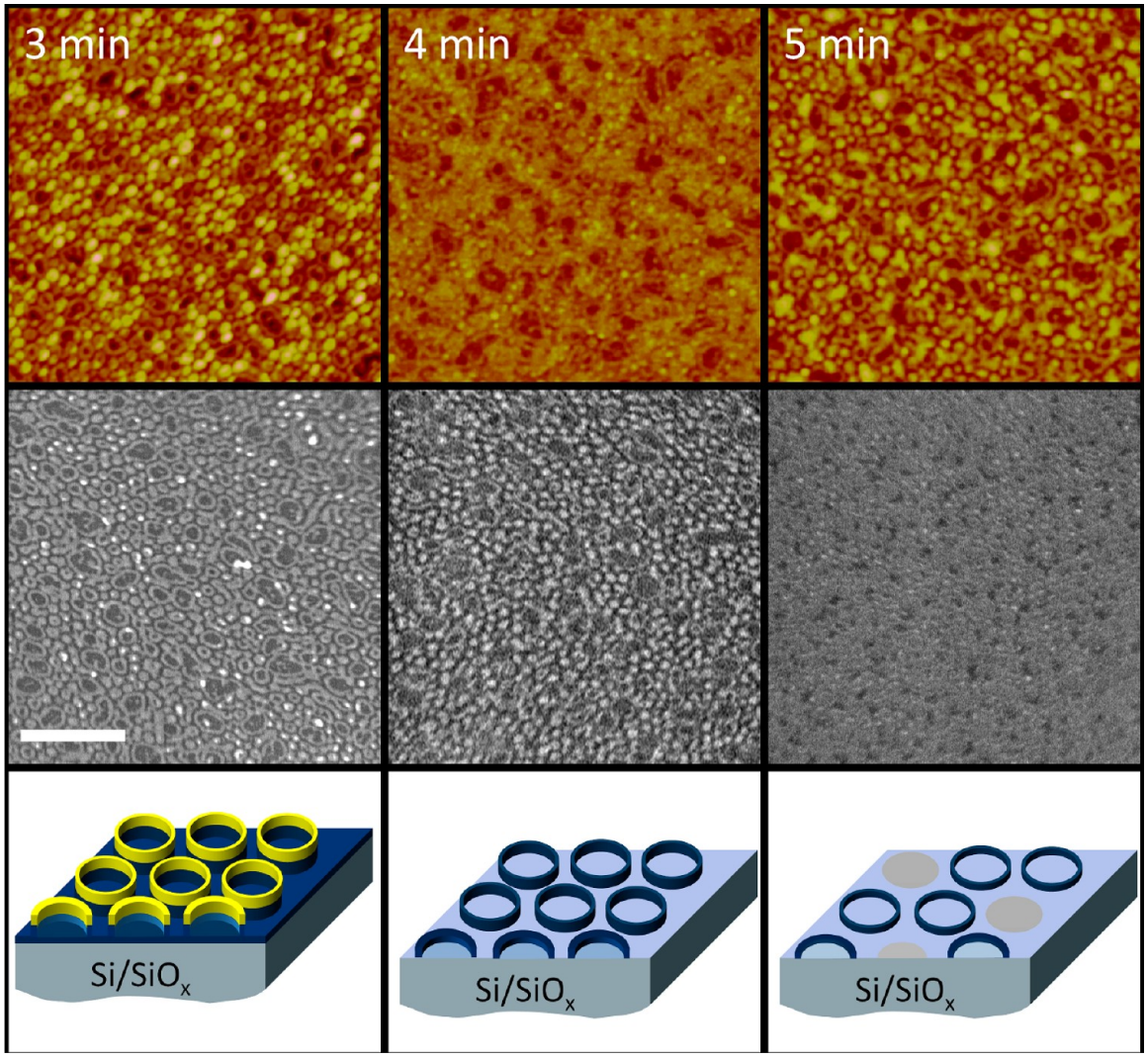

Figure 6. Series of tapping mode AFM (top) and plan view SEM (middle) images of $Ni_{80}Fe_{20}$ nanorings as a function of Ar ion beam mill time at 3, 4, and 5 min with their respective illustrations (similar to Figure 4) below. Scale bar represents 500 nm.

SiO_x rings) the maximum possible ring height from a 52 nm thick PS-PDMS-PLA film would be ~19 nm (see the Supporting Information). However, taking into account the observed change in lateral area before and after O_2 RIE (based on AFM and SEM images described above, the area increases by a factor of ~2, likely due to spreading of PDMS during conversion), the expected height should actually be closer to 9.2 nm, consistent with our cross-sectional SEM data. This result indicates a conversion rate of PDMS to SiO_x during the O_2 RIE process that can be quantitatively understood.

Encouraged by the well-defined SiO_x ring array after O_2 RIE of the PS-PDMS-PLA film, pattern transfer into the underlying 10 nm thick Au layer was attempted using Ar ion beam milling at normal incidence. The expected etch rates (based on witness films of Au and SiO_2) are 10 and 2.5 nm/min (giving a 1 and 4.5 min etch window for Au and SiO_x), respectively.[39] This implies that after one minute of milling the unprotected Au will be removed, leaving behind a significant fraction of residual SiO_x capping layer covering patterned Au rings. Indeed, after 1 min of milling, plan view, as well as cross-sectional (obtained by cryogenically fracturing the sample in liquid N_2) SEM images were obtained, and are shown in Figure 5c and d. Plan view images (Figure 5c) display a high contrast view of ringlike structures that are qualitatively similar to the initial SiO_x ring mask, although the rings are less well defined. The linking material seen between the rings is likely due to resputtering effects during the milling process from both the Au, and possibly the underlying $Ni_{80}Fe_{20}$. The cross-sectional image (Figure 5d) is also revealing, showing nanorings that traverse the entire thickness and have lateral dimensions very similar to that of the original etch mask (Figure 5a). In addition, there is a significant height increase in the individual rings (Figure 5d) when compared to the original SiO_x rings (Figure 5b), giving a strong indication of successful pattern transfer. Height measurements from this image indicate ~22 nm tall rings, approximately twice the height of the original SiO_x rings. This implies that roughly 11 nm of unprotected Au was etched, consistent with the original film thickness of 10 nm. (The etch rate of the underlying $Ni_{80}Fe_{20}$ is very similar to the SiO_x etch mask (~2 nm/min) meaning that little, if any, penetration is likely to have occurred into this layer after 1 min.) Thus, the cross-sectional image displays gold nanorings topped by the remaining SiO_x ring mask. Moreover, viewing the front face of the fracture in the tilted SEM image gives strong indication that the milled pores within and the voids outside the rings clearly

span the entire thickness, further confirming successful pattern transfer.

To demonstrate the versatility of the pattern transfer method, Ar ion beam milling was continued for longer times, continuing through the Au overlayer and patterning the underlying metallic alloy layer. As previously described, the thin films stack is a 10 nm Au capped 10 nm $Ni_{80}Fe_{20}$ layer. Similar to above, the SiO_x ring etch mask was prepared from solvent annealed PS-PDMS-PLA film by first employing a 15 s CF_4 RIE, followed by a 60 s O_2 RIE. Based on etch rates of the various materials, roughly 4 min of additional etch time (beyond the first minute to remove the unprotected Au layer) are possible before the SiO_x etch mask is fully removed via the Ar ion etching. Thus, we can expect the removal of nearly 8−10 nm of the underlying, unprotected alloy film after 5 min of total mill time. Figure 6 shows a series of plan view SEM images of nanorings at various mill times (in 1 min intervals) beyond the initial removal of the Au overlayer, clearly demonstrating successful transfer to the underlying film. Clear definitions of rings structures are seen through 4 min of milling. By 5 min the alloy material is nearly completely removed, leaving only pits and a few residual rings. Charging in the SEM becomes significant by the final image due to exposure of the insulating SiO_2-capped substrate, providing further evidence of penetration through the extent of the film, but also making it difficult to resolve the final structures. To demonstrate further extensibility, the procedure described above was also performed on a 10 nm Au capped 10 nm $Ni_{80}Cr_{20}$ layer ($Ni_{80}Cr_{20}$ mills slightly slower than $Ni_{80}Fe_{20}$). The successful pattern transfer occurs in a nearly identical fashion to the $Ni_{80}Fe_{20}$ layer (see the Supporting Information).

SUMMARY

In summary, a new ABC triblock terpolymer with a core−shell morphology containing the oxidizable PDMS domain as the core−shell midblock, with PLA (minority core) and PS (majority matrix) end blocks was successfully synthesized, confirmed by ^{1}H NMR, SEC, TEM and SAXS. In addition, thin films of the PS-PDMS-PLA were spun cast from chlorobenzene, where AFM and SEM imaging gives results consistent with a core−shell microstructure. By annealing in toluene vapor, well -rdered core−shell cylinders orient perpendicular to the underlying substrate/film. The lateral ordering of these cylinders is maintained through the extent of the film down to the substrate (important for pattern transfer-based lithographic approaches), but leaves a thin PDMS wetting layer at the free surface. Removal of the PDMS wetting layer with CF_4 RIE and subsequent exposure of the film to an O_2 RIE removes the PS matrix and PLA core and converts the PDMS core−shell into an array of SiO_x rings. This procedure was carried out on two metallic stacks, where normal incident Ar ion beam milling successfully removed the unprotected underlying material, giving evidence that the SiO_x ring array acted as a robust etch mask, and resulted in an array of metallic ring structures. By way of cross-sectional SEM images, it is clear that successful pattern transfer occurs, even within the narrow core region. The generality of this method was demonstrated by preparing nanoring arrays of an Au overlayer, as well as $Ni_{80}Fe_{20}$ and $Ni_{80}Cr_{20}$ underlayers. Such ring arrays could find use in a variety of applications, particularly in optoelectronics[12,13,16,40] and the general area of magnetic nanostructures.[10,11,41,42]

ASSOCIATED CONTENT

Supporting Information

Experimental details, including polymer characterization with ^{1}H NMR spectra, SEC traces, as well as additional SEM images of thin-film processing steps and the calculation of ring heights. This material is available free of charge via the Internet at http://pubs.acs.org.

AUTHOR INFORMATION

Corresponding Author

*E-mail: hillmyer@umn.edu.

Author Contributions

‡Both authors contributed equally to this work

Notes

The authors declare no competing financial interest.

ACKNOWLEDGMENTS

This work was supported primarily by the MRSEC Program of the National Science Foundation under Award DMR-0819885. We also acknowledge support from the NSF under DMR-1006370. A.B. thanks G. Theryo for useful discussion.

REFERENCES

(1) Bates, F. S.; Fredrickson, G. H. *Phys. Today* **1999**, *52*, 32.
(2) Matsen, M. W.; Thompson, R. B. *J. Chem. Phys.* **1999**, *111*, 7139.
(3) Bates, F. S.; Fredrickson, G. H. *Annu. Rev. Phys. Chem.* **1990**, *41*, 525.
(4) Park, M.; Harrison, C.; Chaikin, P. M.; Register, R. A.; Adamson, D. H. *Science* **1997**, *276*, 1401.
(5) Fasolka, M. J.; Mayes, A. M. *Annu. Rev. Mater. Res.* **2001**, *31*, 323.
(6) Bailey, T.; Hardy, C.; Epps, T.; Bates, F. *Macromolecules* **2002**, *35*, 7007.
(7) Guo, S.; Rzayev, J.; Bailey, T. S.; Zalusky, A. S.; Olayo-Valles, R.; Hillmyer, M. A. *Chem. Mater.* **2006**, *18*, 1719.
(8) Matveev, K. A.; Larkin, A. I.; Glazman, L. I. *Phys. Rev. Lett.* **2002**, *89*, 096802.
(9) Lévy, L. P.; Dolan, G.; Dunsmuir, J.; Bouchiat, H. *Phys. Rev. Lett.* **1990**, *64*, 2074.
(10) Nam, C.; Ng, B. G.; Castaño, F. J.; Ross, C. A. *J. Appl. Phys.* **2009**, *105*, 033918.
(11) Rothman, J.; Kläui, M.; Lopez-Dias, L.; Vaz, C. A. F.; Bleloch, A.; Bland, J. A. C.; Cui, Z.; Speaks, R. *Phys. Rev. Lett.* **2001**, *86*, 1098.
(12) Aizpurua, J.; Hanarp, P.; Sutherland, D. S.; Käll, M.; Bryant, G. W.; García de Abajo, F. J. *Phys. Rev. Lett.* **2003**, *90*, 057401.
(13) Hao, F.; Nordlander, P.; Sonnefraud, Y.; Van Dorpe, P.; Maier, S. A. *ACS Nano* **2009**, *3*, 643.
(14) Bayati, M.; Patoka, P.; Giersig, M.; Savinova, E. R. *Langmuir* **2010**, *26*, 3549.
(15) Hao, F.; Nordlander, P.; Burnett, M. T.; Maier, S. A. *Phys. Rev. B.* **2007**, *76*, 245417.
(16) Kim, S.; Jung, J.-M.; Choi, D.-G.; Jung, H.-T.; Yang, S.-M. *Langmuir* **2006**, *22*, 7109.
(17) Nordlander, P. *ACS Nano* **2009**, *3*, 488.
(18) Liu, X.; Stamm, M. *Macromol. Rapid Commun.* **2009**, *30*, 1345.
(19) Yin, M.; Cheng, Y.; Liu, M.; Gutmann, J.; Müllen, K. *Angew. Chem., Int. Ed.* **2008**, *47*, 8400.
(20) Wang, L.; Montagne, F.; Hoffmann, P.; Pugin, R. *Chem. Commun.* **2009**, *25*, 3798.
(21) Singh, D. K.; Krotkov, R. V.; Xiang, H.; Xu, T.; Russell, T. P.; Tuominen, M. T. *Nanotechnology* **2008**, *19*, 245305.
(22) Ryu, J.-H.; Park, S.; Kim, B.; Klaikherd, A.; Russell, T. P.; Thayumanavan, S. *J. Am. Chem. Soc.* **2009**, *131*, 9870.
(23) Chao, C.-C.; Ho, R.-M.; Georgopanos, P.; Avgeropoulos, A.; Thomas, E. L. *Soft Matter* **2010**, *6*, 3582.

(24) Chuang, V. P.; Ross, C. A.; Bilalis, P.; Hadjichristidis, N. *ACS Nano* 2008, *2*, 2007.
(25) Jeon, S.; Jang, K.; Lee, S. H.; Park, H.; Sohn, B. *Langmuir* **2008**, *24*, 11137.
(26) Chuang, V. P.; Ross, C. A.; Gwyther, J.; Manners, I. *Adv. Mater.* **2009**, *21*, 3789.
(27) Maheshwari, S.; Tsapatsis, M.; Bates, F. S. *Macromolecules* **2007**, *40*, 6638.
(28) Guo, F.; Jankova, K.; Schulte, L.; Vigil, M. E.; Ndoni, S. *Macromolecules* **2008**, *41*, 1486.
(29) Srividhya, M.; Madhavan, K.; Reddy, B. S. R. *Eur. Polym. J.* **2006**, *42*, 2743.
(30) Due to problems with exact magnification calibrations in AFM imaging, all AFM images in this manuscript are scaled by the center-to-center distances obtained from the accompanying SEM images (i.e., 61.0 nm).
(31) Kubo, T.; Wang, R. F.; Olson, D. A.; Rodwogin, M.; Hillmyer, M. A.; Leighton, C. *Appl. Phys. Lett.* **2008**, *93*, 133112.
(32) *Polymer Handbook*, 4th ed.; Brandrup, J., Immergut, E. H., Grulke, E. A., Eds.; Wiley: New York, 1999.
(33) Ringard-Lefebvre, C.; Baszkin, A. *Langmuir* **1994**, *10*, 2367−2381.
(34) Kim, S. H.; Misner, M. J.; Xu, T.; Kimura, M.; Russell, T. P. *Adv. Mater.* **2004**, *16*, 226−231.
(35) Kim, S. H.; Misner, M. J.; Russell, T. P. *Adv. Mater. (Weinheim, Ger.)* **2004**, *16*, 2119−2123.
(36) Jung, Y.; Ross, C. *Nano Lett.* **2007**, *7*, 2046−2050.
(37) Williams, K. R.; Gupta, K.; Wasilik, M. *J. Microelectromech. Syst.* **2003**, *12*, 761.
(38) *CRC Handbook of Chemistry and Physics*, 91st ed; Haynes, W. M., Ed.; CRC Press/Taylor and Francis, Boca Raton, FL, 2011.
(39) Etch rates established on uniform films at the University of Minnesota Nanofabrication Center.
(40) Hill, M. T.; et al. *Nature* **2004**, *432*, 206−209.
(41) Castaño, F. J.; Morecroft, D.; Jung, W.; Ross, C. A. *Phys. Rev. Lett.* **2005**, *95*, 137201.
(42) Wen, Z. C.; Wei, H. X.; Han, X. F. *Appl. Phys. Lett.* **2007**, *91*, 122511.